UC Riverside
UC Riverside Previously Published Works

Title

Myeloid-specific deficiency of pregnane X receptor decreases atherosclerosis in LDL receptor-deficient mice [S]

Permalink

https://escholarship.org/uc/item/10b3j23n

Journal

Journal of Lipid Research, 61(5)

ISSN

0022-2275

Authors

Sui, Yipeng
Meng, Zhaojie
Park, Se-Hyung
et al.

Publication Date

2020-05-01

DOI

10.1194/jlr.ra119000122

Copyright Information

Peer reviewed

Myeloid-specific deficiency of pregnane X receptor decreases atherosclerosis in LDL receptor-deficient mice[S]

Yipeng Sui,* Zhaojie Meng,*,† Se-Hyung Park,* Weiwei Lu,* Christopher Livelo,† Qi Chen,† Tong Zhou,§ and Changcheng Zhou[1],*,†

Department of Pharmacology and Nutritional Sciences,* University of Kentucky, Lexington, KY 40536; Division of Biomedical Sciences,† School of Medicine, University of California, Riverside, CA 92521; and Department of Physiology and Cell Biology,§ Reno School of Medicine, University of Nevada, Reno, NV 89557

Abstract The pregnane X receptor (PXR) is a nuclear receptor that can be activated by numerous drugs and xenobiotic chemicals. PXR thereby functions as a xenobiotic sensor to coordinately regulate host responses to xenobiotics by transcriptionally regulating many genes involved in xenobiotic metabolism. We have previously reported that PXR has pro-atherogenic effects in animal models, but how PXR contributes to atherosclerosis development in different tissues or cell types remains elusive. In this study, we generated an LDL receptor-deficient mouse model with myeloid-specific PXR deficiency ($PXR^{\Delta Mye}LDLR^{-/-}$) to elucidate the role of macrophage PXR signaling in atherogenesis. The myeloid PXR deficiency did not affect metabolic phenotypes and plasma lipid profiles, but $PXR^{\Delta Mye}LDLR^{-/-}$ mice had significantly decreased atherosclerosis at both aortic root and brachiocephalic arteries compared with control littermates. Interestingly, the PXR deletion did not affect macrophage adhesion and migration properties, but reduced lipid accumulation and foam cell formation in the macrophages. PXR deficiency also led to decreased expression of the scavenger receptor CD36 and impaired lipid uptake in macrophages of the $PXR^{\Delta Mye}LDLR^{-/-}$ mice. Further, RNA-Seq analysis indicated that treatment with a prototypical PXR ligand affects the expression of many atherosclerosis-related genes in macrophages in vitro.[jlr] These findings reveal a pivotal role of myeloid PXR signaling in atherosclerosis development and suggest that PXR may be a potential therapeutic target in atherosclerosis management.—Sui, Y., Z. Meng, S-H. Park, W. Lu, C. Livelo, Q. Chen, T. Zhou, and C. Zhou. **Myeloid-specific deficiency of pregnane X receptor decreases atherosclerosis in LDL receptor-deficient mice.** *J. Lipid Res.* 2020. **61:** 696–706.

Supplementary key words macrophages • cluster of differentiation 36 • foam cells • lipids • cardiovascular disease • xenobiotic sensor • lipid homeostasis • transcriptome • low density lipoprotein

Despite major advances in developing diagnostic techniques and effective treatments, atherosclerotic CVD is still the leading cause of mortality and morbidity worldwide (1). Atherosclerosis is a complex chronic disease involving the interaction of genetic and environmental factors over many years. Nuclear receptors are one of the largest groups of transcriptional factors that function as master regulators of many genes involved in metabolic control, including fat, glucose, cholesterol, bile acid, and xenobiotic metabolism (2, 3). Several nuclear receptors, including LXR and PPARs, that play key roles in lipid homeostasis have been demonstrated to regulate atherosclerosis development in multiple animal models (4, 5).

The pregnane X receptor (PXR) is a unique nuclear receptor that can be activated by numerous endogenous hormones, dietary steroids, pharmaceutical agents, and xenobiotic chemicals (6–9). PXR is expressed at high levels in liver and intestine where it can regulate many genes required for xenobiotic metabolism, including cytochrome P450 (CYP) enzymes (e.g., CYP3A4), conjugating enzymes (e.g., glutathione transferase), and ABC family transporters (e.g., multidrug resistance 1) (7–10). Because it was first identified in 1998, the role of PXR in the regulation of xenobiotic metabolism has been extensively studied by many laboratories including ours, and PXR has also been established as a xenobiotic sensor to mediate xenobiotic responses (7–9).

In addition to xenobiotic metabolism, recent studies have discovered novel functions of PXR in lipid homeostasis

and atherogenesis (9, 11–14). For example, we previously demonstrated that PXR has pro-atherogenic effects in mouse models (11, 12) and found that ligand-mediated PXR activation increased plasma total cholesterol levels and atherogenic lipoproteins such as LDL levels in wild-type mice (11, 13–16). Interestingly, chronic activation of PXR also significantly increased atherosclerosis in atherosclerosis-prone ApoE$^{-/-}$ mice (11). To further study the role of PXR in atherosclerosis, we also generated PXR$^{-/-}$ApoE$^{-/-}$ double knockout mice and found that whole-body PXR deficiency significantly decreased atherosclerosis in PXR$^{-/-}$ApoE$^{-/-}$ mice without affecting the plasma lipid profile (12).

In addition to liver and intestine, PXR is also expressed in immune cells including T cells, B cells, and macrophages (11, 17–22). Macrophages play a key role in atherosclerosis initiation and development, and accumulation of lipid-loaded macrophages is a hallmark of atherosclerosis (23, 24). While our previous studies indicate that PXR may regulate macrophage functions to affect atherosclerosis development (11, 12), the role of macrophage PXR in atherosclerosis remains obscure partly due to the lack of conditional PXR knockout mice.

To define the functions of macrophage-derived PXR in atherogenesis, we developed a novel LDLR-deficient mouse model with myeloid-specific PXR deficiency (PXR$^{\Delta Mye}$LDLR$^{-/-}$). Here, we demonstrate that deficiency of myeloid PXR decreases atherosclerosis in LDLR$^{-/-}$ mice, which is likely due to reduced macrophage lipid uptake and foam cell formation.

MATERIALS AND METHODS

Animals

Mice carrying PXR flox alleles (PXR$^{F/F}$) were generated by using mouse embryonic stem cell clones containing conditional PXR flox alleles (C57BL/6N background) as previously described (13, 14). PXR$^{F/F}$ mice were then backcrossed to C57BL/6J mice for at least six generations prior to further crossing. Myeloid-specific PXR knockout (PXR$^{\Delta Mye}$) mice were generated by crossing PXR$^{F/F}$ mice with LysM-Cre transgenic mice (Jackson Laboratory) (25, 26). To increase susceptibility to atherosclerosis development, the PXR$^{\Delta Mye}$ mice were crossed to LDLR$^{-/-}$ mice (Jackson Laboratory) to generate PXR$^{\Delta Mye}$LDLR$^{-/-}$ and PXR$^{F/F}$LDLR$^{-/-}$ mice. Because PXR$^{F/F}$ and LysM-Cre transgenic mice have mixed C57BL/6J and C57BL/6N background, PXR$^{\Delta Mye}$LDLR$^{-/-}$ and PXR$^{F/F}$LDLR$^{-/-}$ littermates were used in this study. All experimental mice had PXR$^{F/F}$ LDLR$^{-/-}$ double-mutant background, and PXR$^{\Delta Mye}$LDLR$^{-/-}$ mice carried heterozygous knock-in for LysM-Cre. For atherosclerosis study, 4-week-old male PXR$^{\Delta Mye}$LDLR$^{-/-}$ and PXR$^{F/F}$ LDLR$^{-/-}$ littermates were fed a low-fat and low-cholesterol semi-synthetic AIN76a diet (27, 28) for 12 weeks until euthanasia at 16 weeks of age. Body composition was measured by EchoMRI (Echo Medical System) and an intraperitoneal glucose tolerance test was performed as previously described (29, 30). All animals were housed in a pathogen-free environment with a light-dark cycle under a protocol approved by the University of Kentucky Institutional Animal Care and Use Committee.

Plasma analysis

Plasma total cholesterol and triglyceride concentrations were determined enzymatically by colorimetric methods as described previously (12, 26). FPLC was used to analyze plasma lipoprotein cholesterol distributions in the pooled plasma samples from multiple mice (n = 6) (12, 26).

Quantification of atherosclerosis

The atherosclerotic lesions were quantified as previously described (12, 26). To quantify the lesion areas at the aortic root, OCT-compound-embedded hearts were sectioned at a 12 μm thickness keeping all three valves of the aortic root in the same plane, and stained with Oil Red O as described before (12, 26). To quantify atherosclerosis at the brachiocephalic artery (BCA), the OCT-embedded BCAs were sectioned from distal to proximal at a thickness of 10 μm. Atherosclerotic lesions lumenal to the internal elastic lamina were quantified in three equidistant Oil Red O-stained sections 200, 400, and 600 μm proximal from the branching point of the BCA into the carotid and subclavian arteries (12, 26).

Macrophage isolation and function assays

Macrophages were isolated as previously described (26, 31). Mice were injected intraperitoneally with 1 ml of 3% thioglycollate, and peritoneal macrophages (PMs) were collected with PBS 4 days later. The PMs from each genotype were allowed to attach to coverslips for 4 h and stained with Oil Red O/hematoxylin. Cells containing lipid droplets (>10) were counted as foam cells. Bone marrow-derived macrophages (BMMs) were isolated from the femurs and tibias of the mice and cultured in DMEM medium supplemented with 10 ng/ml recombinant mouse macrophage colony-stimulating factor (Invitrogen) for 8–10 days. For adhesion assay, calcein acetoxymethyl-labeled PMs were incubated with primary porcine endothelial cells (ECs) (a gift from Dr. Bernhard Hennig at the University of Kentucky). The attached cells were fixed and counted via microscope. Migration assays were performed using transwells with 8 μm pore polycarbonate membrane inserts (Corning). Macrophages with serum-free medium were seeded on the transwell filters, and the lower chambers were filled with the complete medium including 10% FBS (Sigma-Aldrich) as a chemoattractant. After 16 h, the cells were removed from the upper surface of the insert using Q-Tips. The membranes were fixed with 1% glutaraldehyde (Sigma), stained with hematoxylin (Leica), and mounted on the slides using glycerol gelatin. Hematoxylin-stained cells were counted under the microscope. For lipid uptake assay, macrophages were incubated with serum-free DMEM containing 100 μg/ml of oxidized LDL (oxLDL) (Biomedical Technologies) for 24 h, followed by staining with Oil Red O/hematoxylin. The number of foam cells was counted.

RNA isolation and quantitative real-time PCR analysis

Total RNA was isolated from mouse tissues or cells using TRIzol reagent (Thermo Fisher Scientific, 15596026) and QPCR was performed using gene-specific primers and the SYBR Green PCR kit (Bio-Rad, 170-8886) as previously described (32). The sequences of primer sets used in this study are listed in supplemental Table S2.

RNA sequencing and data analysis

PMs were isolated from PXR$^{F/F}$LDLR$^{-/-}$ and PXR$^{\Delta Mye}$LDLR$^{-/-}$ mice. Cells were attached to cell culture plates for 4 h and were then treated with 20 μM mouse PXR ligand pregnenolone 16α-carbonitrile (PCN) or vehicle control (DMSO) for 12 h. Total RNA was extracted, and RNA integrity was confirmed using a dual Agilent 2100 bioanalyzer (Agilent Technologies Inc., Santa Clara, CA). The creation of cDNA libraries and sequencing was performed

using the Illumina standard operation pipeline as previously described (33, 34). For data analysis, we applied the Sailfish tool (35) to quantify the mRNA expression from the raw sequencing data, using the Ensembl (36) mouse gene annotation (GRCm38). Transcript per million reads (TPM) was used as the unit of mouse gene expression level. We then used the edgeR algorithm (37) to compare the groupwise transcriptomic pattern. We also applied the TMM algorithm implemented in the edgeR package to perform reads count normalization and effective library size estimation. Group-wise differential expression was estimated by the likelihood ratio test implicated in the edgeR package. The genes with a false discovery rate (FDR) of <5% and a fold change (FC) of >1.5 were deemed differentially expressed. All RNA sequencing (RNA-Seq) datasets have been deposited in the Gene Expression Omnibus (GSE145719). We further performed Gene Ontology (GO) analysis upon the differentially expressed genes (DEGs) using the definition from the GO project (38).

Western blotting

Western blotting was performed as previously described (39). Briefly, the cells or tissues were homogenized with Bullet Blender (Next Advance BBX24, Averill Park, NY) in 0.5 ml of ice-cold lysis buffer (Cell Signaling Technology, 9803) containing protease inhibitor cocktails (Roche, 11836153001) and phosphatase inhibitor cocktails (Sigma-Aldrich, P5726 and P0044). After homogenization, lysates were centrifuged at 16,000 g for 15 min at 4°C to collect the supernatant. Protein concentrations were measured by using a bicinchoninic acid protein assay kit (Thermo Fisher Scientific, 23225). Proteins were resolved on SDS-PAGE and then transferred to nitrocellulose membrane. The membrane was blocked in PBS solution with 0.05% Tween 20 (PBST, pH 7.4) containing 5% nonfat dry milk (Bio-Rad, 170-6404) for 1–3 h and then incubated with goat anti-PXR antibodies (1:500, Santa Cruz Biotechnology, sc-7739) in PBST containing 5% BSA at 4°C overnight. After the incubation, the membrane was washed four times with PBST and incubated with HRP-conjugated rabbit anti-goat secondary antibodies (1:2,000; Sigma-Aldrich, A8919) in PBST with 5% nonfat dry milk for 1 h at room temperature. After subsequent three-time washing in PBST, the membrane was washed once in PBS and developed using Pierce ECL Western blotting substrate (Thermo Fisher Scientific, 32209) and exposed to CL-XPosure films (Thermo Fisher Scientific, 34099).

Immunohistochemistry

Immunohistochemistry was performed on 12 μm sections of aortic roots freshly embedded in OCT. The slides were fixed in ice-cold acetone for 15 min and permeabilized with PBS + 0.1% Triton X-100 (TPBS) for 15 min and blocked with TPBS containing 5% BSA (Sigma-Aldrich, A9647) for 1 h at room temperature. The sections were then incubated with rat anti-CD68 antibody (1:100; AbD Serotec, MCA1957), rabbit anti-PXR antibody (1:50; Santa Cruz Biotechnology, SC25381), rabbit anti-αSMA antibody (1:200; Abcam, ab5694), or rat anti-mouse CD36 antibody (1:100; AbD Serotec, MCA2683) at 4°C overnight. The slides were rinsed with PBS and incubated with corresponding secondary antibodies (1:500; Life Technologies). The nuclei were stained by mounting the slides with DAPI medium (Vector Laboratories). Images were acquired under a Nikon fluorescence microscope (Nikon). For collagen staining, Masson's Trichrome staining was performed following the standard procedure (40).

Statistical analysis

All data except the high-throughput sequencing data are presented as the mean ± SEM. Individual pairwise comparisons were analyzed by two-sample two-tailed Student's t-test unless otherwise noted, with $P < 0.05$ regarded as significant using GraphPad Prism. Two-way ANOVA was done using SigmaPlot 13.0 when multiple comparisons were made followed by a Bonferroni multiple comparisons test. Numbers of mice used are listed in figure legends.

<div style="text-align:center">RESULTS</div>

Generation of myeloid-specific PXR-deficient LDLR$^{-/-}$ mice

To investigate the role of PXR in macrophage functions, we generated myeloid-specific PXR knockout mice (PXR$^{\Delta Mye}$) by crossing PXR flox mice (PXR$^{F/F}$) (13, 14) with LysM-Cre transgenic mice (25, 31) (supplemental Fig. S1A). To study the functions of macrophage PXR in atherosclerosis, PXR$^{\Delta Mye}$ mice were crossed with LDLR$^{-/-}$ mice to generate PXR$^{\Delta Mye}$LDLR$^{-/-}$ mice. PCR analysis using genomic DNA demonstrated that the Cre recombination was specific to the PMs and BMMs (supplemental Fig. S1B). QPCR assay suggested that the mRNA levels of PXR significantly descended in both PMs and BMMs but not in other major organs of PXR$^{\Delta Mye}$LDLR$^{-/-}$ mice compared with PXR$^{F/F}$LDLR$^{-/-}$ littermates (**Fig. 1A**). Consistently, the protein levels of PXR were also decreased in macrophages but not in liver of PXR$^{\Delta Mye}$LDLR$^{-/-}$ mice (Fig. 1B). These results demonstrated the specific and efficient PXR deletion in macrophages of PXR$^{\Delta Mye}$LDLR$^{-/-}$ mice.
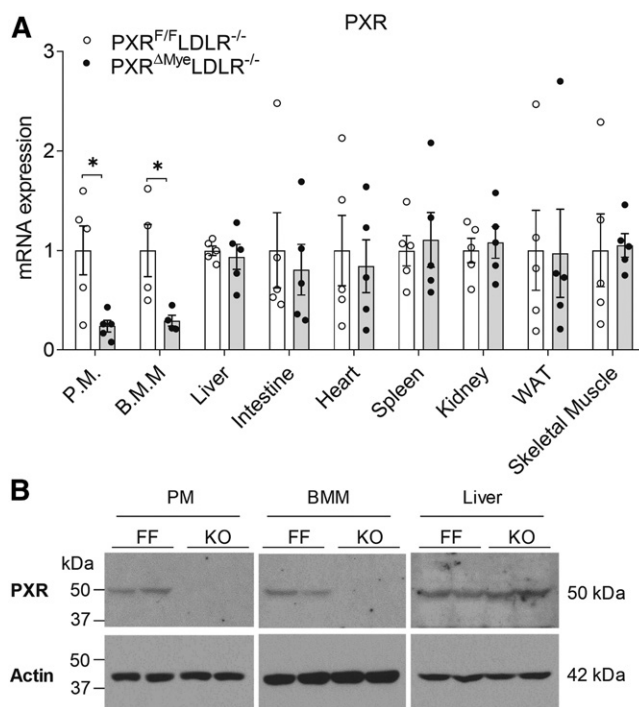

Fig. 1. Generation of LDLR$^{-/-}$ mice with myeloid-specific PXR deficiency. A: mRNA levels of PXR in PMs, BMMs, and the other major tissues of PXR$^{F/F}$LDLR$^{-/-}$ and PXR$^{\Delta Mye}$LDLR$^{-/-}$ mice (n = 4–5, *$P < 0.05$). B: Immunoblotting for PXR proteins in PMs, BMMs, and liver of PXR$^{F/F}$LDLR$^{-/-}$ and PXR$^{\Delta Mye}$LDLR$^{-/-}$ mice.

Deficiency of myeloid PXR does not affect metabolic phenotypes and plasma lipid profiles in LDLR$^{-/-}$ mice

To investigate the role of macrophage PXR in atherosclerosis development, 4-week-old male PXR$^{\Delta Mye}$LDLR$^{-/-}$ and PXR$^{F/F}$LDLR$^{-/-}$ littermates were fed a modified semisynthetic low-fat (4.3%) and low-cholesterol (0.02%) AIN76 diet (27). This modified diet has been successfully used by us and others to induce atherosclerosis in LDLR$^{-/-}$ or ApoE$^{-/-}$ mice without eliciting obesity and associated metabolic disorders (12, 27, 28, 41). To determine whether deficiency of myeloid PXR affects weight gain and body composition, the body weight was measured weekly and the body composition was measured by EchoMRI. Deficiency of myeloid PXR did not affect the growth curve (**Fig. 2A**) and the body composition including fat and lean mass in PXR$^{\Delta Mye}$LDLR$^{-/-}$ mice (Fig. 2B). Further, myeloid PXR deficiency did not affect the weight of major organs including liver, kidney, and brown adipose tissue in LDLR$^{-/-}$ mice at the time of euthanasia (Fig. 2C).

In addition to similar body weight and composition, PXR$^{\Delta Mye}$LDLR$^{-/-}$ and PXR$^{F/F}$LDLR$^{-/-}$ mice had similar plasma glucose levels (Fig. 2D), and glucose tolerance tests also demonstrated that myeloid PXR deficiency did not alter glucose tolerance in PXR$^{\Delta Mye}$LDLR$^{-/-}$ mice (Fig. 2D). Further, myeloid PXR deletion did not alter plasma total cholesterol and triglyceride levels (**Fig. 3A**, B) and FPLC analysis also showed a similar cholesterol distribution pattern between PXR$^{\Delta Mye}$LDLR$^{-/-}$ and PXR$^{F/F}$LDLR$^{-/-}$ mice (Fig. 3C).

Deficiency of PXR in macrophages decreased atherosclerosis in LDLR$^{-/-}$ mice

Although deficiency of myeloid PXR did not affect metabolic phenotypes and plasma lipid levels, quantification of cross-sectional lesion areas at the aortic root revealed that PXR$^{\Delta Mye}$LDLR$^{-/-}$ mice had 50% decreased lesion size (29,214 ± 3,669 μm^2) as compared with PXR$^{F/F}$LDLR$^{-/-}$ littermates (58,189 ± 9,692 μm^2) (**Fig. 4A**). Further, the lesional areas at the BCA were decreased by 28% in PXR$^{\Delta Mye}$LDLR$^{-/-}$ mice (1,574 ± 175 μm^2) as compared with PXR$^{F/F}$LDLR$^{-/-}$ mice (2,179 ± 190 μm^2) (Fig. 4B). To determine whether myeloid PXR ablation affected atherosclerotic lesion composition, we next examined the collagen, smooth muscle cells (SMCs), and macrophages inside the lesion area by immunostaining of macrophage marker, CD68, and SMC marker, α-smooth muscle actin (α-SMA), or Masson's Trichrome staining. The results demonstrated that PXR$^{\Delta Mye}$LDLR$^{-/-}$ mice had decreased macrophage contents but similar SMC and collagen contents within lesions as compared with PXR$^{F/F}$LDLR$^{-/-}$ littermates (**Fig. 5A**–C). Thus, myeloid PXR deficiency significantly decreased atherosclerosis and macrophage contents in LDLR$^{-/-}$ mice without altering metabolic functions.

Ablation of PXR reduces CD36 expression and macrophage foam cell formation

To determine whether PXR signaling regulates macrophage functions related to atherosclerosis development, we first investigated the effects of PXR deficiency on macrophage adhesion and migration properties. Incubation of freshly isolated PMs with primary ECs showed that ablation of PXR did not affect adhesion of macrophages to ECs (supplemental Fig. S2). We also examined the effects of PXR deficiency on macrophage migration by transwell assay. As shown in supplemental Fig. S3, PXR deficiency did not affect macrophage migration ability either.

Accumulation of lipid-loaded macrophages is a hallmark of atherosclerosis (23). We have previously demonstrated that PXR can affect lipid accumulation and foam cell formation in macrophages of ApoE$^{-/-}$ mice (11, 12). We then performed Oil Red O staining to assess neutral lipid levels in freshly isolated PMs of PXR$^{F/F}$LDLR$^{-/-}$ and PXR$^{\Delta Mye}$LDLR$^{-/-}$ mice. Consistently, deficiency of PXR substantially reduced the lipid accumulation and foam cell formation in PMs of PXR$^{\Delta Mye}$LDLR$^{-/-}$ mice (**Fig. 6A**, B). Gene expression analysis demonstrated that PXR ablation significantly decreased the expression levels of scavenger receptor CD36 that plays a key role in macrophage lipid

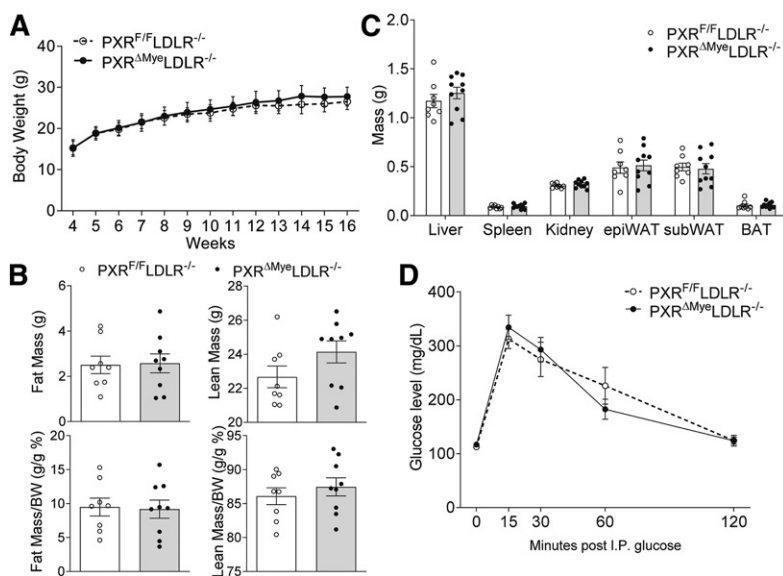**Fig. 2.** Deficiency of myeloid PXR does not affect body weight and glucose tolerance in LDLR$^{-/-}$ mice. Four-week-old male PXR$^{F/F}$LDLR$^{-/-}$ and PXR$^{\Delta Mye}$LDLR$^{-/-}$ littermates were fed a semi-synthetic AIN76a diet containing 0.02% cholesterol for 12 weeks. Growth curve (A), fat and lean mass (B), major organ weight (C), and glucose tolerance (D) were measured (n = 7–12).
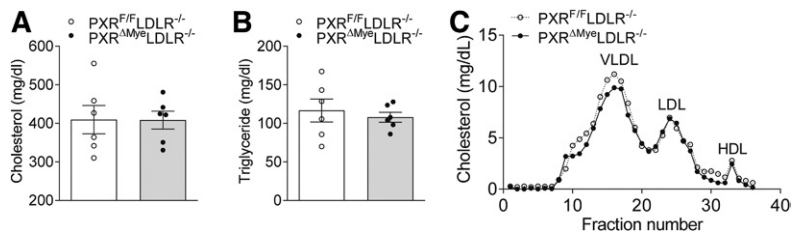
Fig. 3. Deletion of PXR in myeloid cells has no effects on plasma lipid profiles in LDLR$^{-/-}$ mice. Four-week-old male PXR$^{F/F}$LDLR$^{-/-}$ and PXR$^{\Delta Mye}$LDLR$^{-/-}$ littermate mice were fed an AIN76a diet for 12 weeks. The plasma levels of cholesterol (A) and triglyceride (B) were measured (n = 6), and plasma cholesterol distribution (C) was analyzed by FPLC.

uptake and foam cell formation (Fig. 6C) (9, 42, 43). However, the expression levels of another scavenger receptor, SR-A, and ABC transporters, ABCA1 and ABCG1, were comparable in macrophages of PXR$^{F/F}$LDLR$^{-/-}$ and PXR$^{\Delta Mye}$LDLR$^{-/-}$ mice (Fig. 6C). Consistent with decreased macrophage CD36 expression, immunofluorescence staining showed that CD36 proteins were also decreased in the atherosclerotic lesions of PXR$^{\Delta Mye}$LDLR$^{-/-}$ mice (**Fig. 7A**, B). Thus, deficiency of PXR decreased macrophage and lesional CD36 expression and reduced macrophage foam cell formation in PXR$^{\Delta Mye}$LDLR$^{-/-}$ mice.

Because CD36 mediates macrophage uptake of oxLDL, which has been considered as the important atherogenic LDL (42), we then performed oxLDL uptake assays in control and PXR-deficient macrophages. As expected, the uptake of oxLDL was significantly decreased in PMs of PXR$^{\Delta Mye}$LDLR$^{-/-}$ mice as compared with those of PXR$^{F/F}$LDLR$^{-/-}$ mice (**Fig. 8A**, B). In addition to PMs, deficiency of PXR also decreased CD36 expression and oxLDL uptake in BMMs of PXR$^{\Delta Mye}$LDLR$^{-/-}$ mice (supplemental Fig. S4). These results suggest that PXR-mediated CD36 expression regulates foam cell formation in vitro.

PXR ligand treatment affects atherosclerosis-related gene expression in macrophages in vitro

To further explore the role of PXR signaling in regulating the macrophage transcriptome related to atherogenesis, PMs were isolated from PXR$^{F/F}$LDLR$^{-/-}$ and PXR$^{\Delta Mye}$LDLR$^{-/-}$ mice and then treated with vehicle control or a prototypical PXR ligand, PCN (9, 11), for RNA-Seq analysis. We found that PCN treatment can significantly induce 439 DEGs in macrophages of PXR$^{F/F}$LDLR$^{-/-}$ mice with a FDR of <5% and a FC of >1.5 as a cut-off threshold (**Fig. 9A**). The volcano plot also showed the distribution of DEGs, with 121 upregulated and 318 downregulated genes. By contrast, PCN only induced 38 DEGs in PXR-deficient macrophages (Fig. 9A, right panel), indicating the important role of PXR in mediating PCN's impact on the macrophage

transcriptome. GO analysis of those DEGs in control macrophages revealed that DEGs were enriched in several biological processes that may contribute to atherogenesis (Fig. 9B). For example, lipid metabolic, cholesterol biosynthetic, inflammatory response, and positive regulation of cytokine secretion processes were significantly affected by PCN treatment in macrophages of PXR$^{F/F}$LDLR$^{-/-}$ mice. Many of those genes in lipid metabolism (e.g., Npc1l1, Jazf1, Sphk1, Hsd17b1, and Sorl1) and inflammatory responses (e.g., Itgb6, Ccl2, Ccl3, Clec4e, Tnfrsf14, Ccr2, Tlr1, Tlr3, and Tlr11) were regulated by PCN in a PXR-dependent manner (Fig. 9C, supplemental Table S1). Further, we also checked the CD36 gene expression in control and PXR-deficient macrophages. Consistent with our in vivo data, CD36 mRNA levels were significantly decreased by PXR deficiency in macrophages of PXR$^{\Delta Mye}$LDLR$^{-/-}$ mice as compared with those of PXR$^{F/F}$LDLR$^{-/-}$ mice (supplemental Table S1). However, PCN treatment did not further affect CD36 expression in vitro, which is likely due to the different in vitro and in vivo conditions as well as the selected PCN dosage and treatment period. Collectively, these results suggest that PXR signaling may affect multiple processes of lipid homeostasis and inflammatory responses in macrophages that contribute to atherosclerosis development.

DISCUSSION

As a xenobiotic sensor, the role of PXR in xenobiotic and drug metabolism has been well defined. Recent studies from us and other groups have revealed novel functions of PXR beyond xenobiotic metabolism, and emerging evidence suggests that PXR may also play an important role in regulating lipid homeostasis and atherosclerosis (9). For example, we have previously demonstrated the pro-atherogenic effects of PXR signaling in ApoE$^{-/-}$ mice and found that whole-body PXR deficiency significantly decreases atherosclerosis in
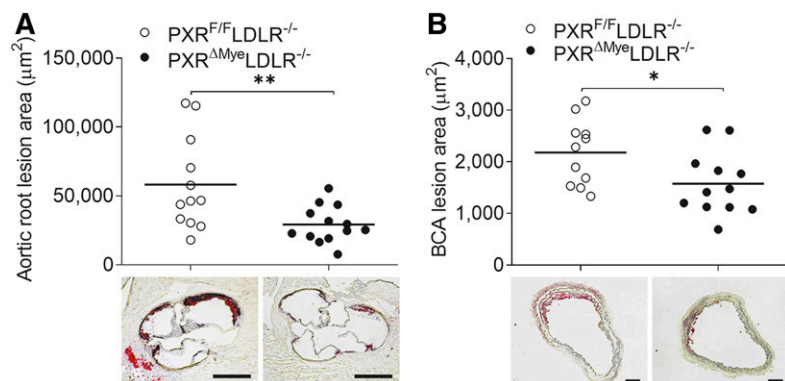

Fig. 4. Deficiency of myeloid PXR decreases atherosclerosis in LDLR$^{-/-}$ mice. Four-week-old male PXR$^{F/F}$LDLR$^{-/-}$ and PXR$^{\Delta Mye}$LDLR$^{-/-}$ littermate mice were fed an AIN76a diet for 12 weeks. Quantitative analysis of the atherosclerotic lesion area at the aortic root (A) and BCA (B) of PXR$^{F/F}$LDLR$^{-/-}$ and PXR$^{\Delta Mye}$LDLR$^{-/-}$ mice (n = 11–13; *$P < 0.05$, **$P < 0.01$). Representative images of Oil Red O-stained sections from each genotype are displayed below the quantification data. Scale bars, 500 μm (A) and 100 μm (B).
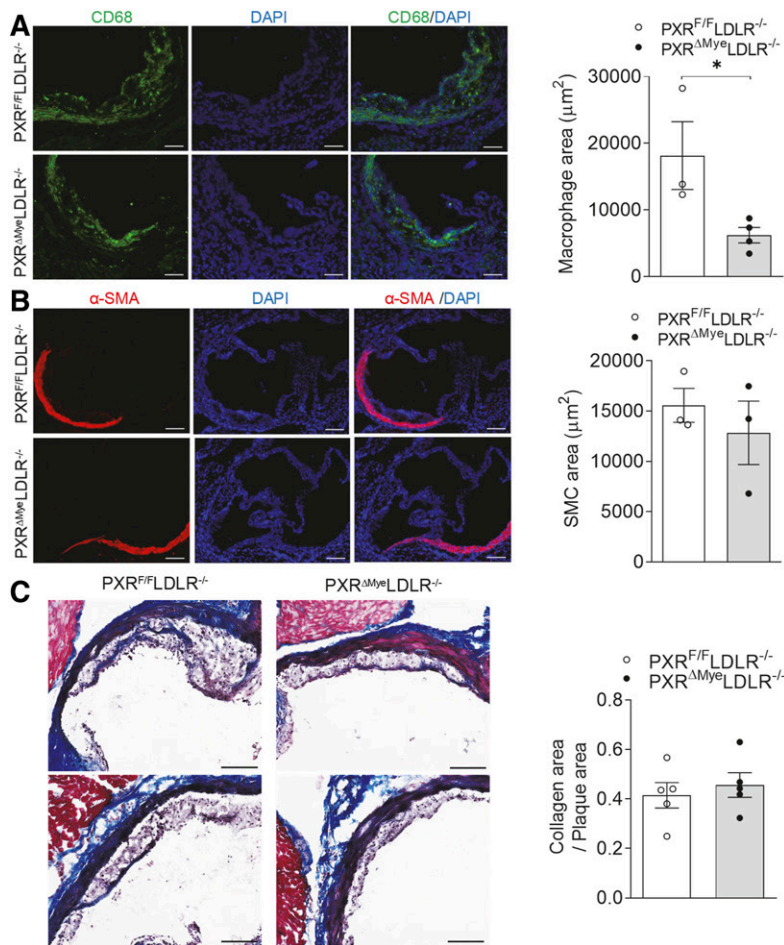
Fig. 5. Ablation of PXR reduces macrophage contents without affecting SMC and collagen contents in atherosclerotic lesions of LDLR$^{-/-}$ mice. Four-week-old male PXR$^{F/F}$LDLR$^{-/-}$ and PXR$^{\Delta Mye}$LDLR$^{-/-}$ littermate mice were fed an AIN76a diet for 12 weeks. Representative images and quantification data of CD68 (A) and α-SMA (B) immunofluorescence staining, and Masson's Trichrome staining (C) at the aortic root of PXR$^{F/F}$LDLR$^{-/-}$ and PXR$^{\Delta Mye}$LDLR$^{-/-}$ mice (n = 3–5, *$P < 0.05$; scale bars, 100 μm).

ApoE$^{-/-}$ mice (12). PXR is expressed in macrophages, but the role of macrophage PXR signaling in atherosclerosis remains elusive. In the current study, we generated novel myeloid-specific PXR-deficient LDLR$^{-/-}$ mice and demonstrated, for the first time, that deficiency of myeloid PXR significantly reduced atherosclerosis in LDLR$^{-/-}$ mice. Myeloid PXR deficiency did not affect plasma lipid profiles but reduced macrophage lipid uptake and foam cell formation, which likely contribute to the decreased atherosclerosis development in those mice.
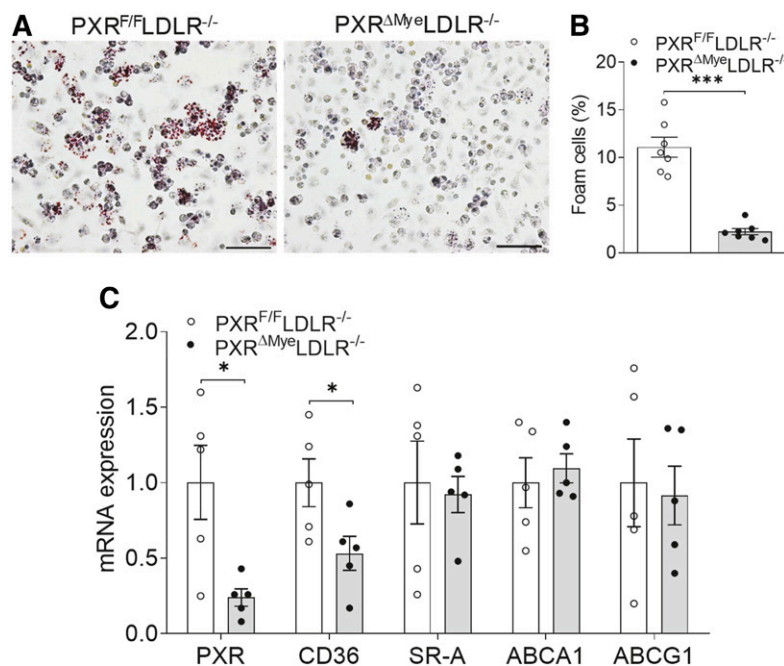
Fig. 6. Deficiency of PXR reduces foam cell formation and CD36 expression in macrophages of PXR$^{\Delta Mye}$LDLR$^{-/-}$ mice. A: Freshly isolated PMs from PXR$^{F/F}$LDLR$^{-/-}$ and PXR$^{\Delta Mye}$LDLR$^{-/-}$ mice fed an AIN76a diet for 12 weeks were stained with Oil Red O and hematoxylin (scale bars, 100 μm). B: Foam cell quantification from PMs in studies described in panel A (n = 7, ***$P < 0.001$). C: Total RNAs were isolated from freshly isolated PMs of PXR$^{F/F}$LDLR$^{-/-}$ and PXR$^{\Delta Mye}$LDLR$^{-/-}$ mice, and the expression levels of the indicated genes were analyzed by QPCR (n = 5, *$P < 0.05$).

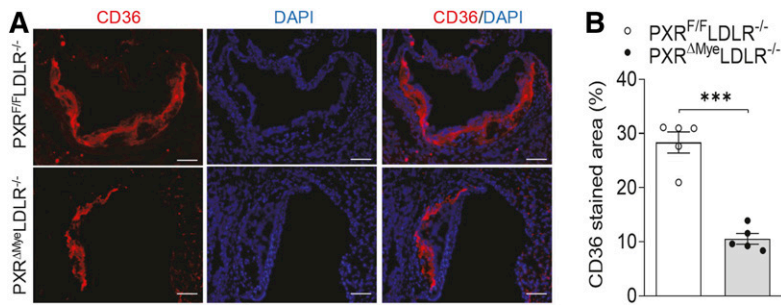**Fig. 7.** Deficiency of myeloid PXR decreases atherosclerotic lesional CD36 expression in PXR$^{\Delta Mye}$LDLR$^{-/-}$ mice. A: Sections of atherosclerotic lesions at the aortic root of PXR$^{F/F}$LDLR$^{-/-}$ and PXR$^{\Delta Mye}$LDLR$^{-/-}$ mice were stained with anti-mouse CD36 primary antibodies, followed by fluorescein-labeled secondary antibodies. The nuclei were stained with DAPI (blue). Scale bars, 100 μm. B: Quantification data of CD36 immunofluorescence staining (n = 5, ***$P< 0.001$).

Macrophages play a central role in atherosclerosis initiation and progression. The innate immune response cell monocytes are recruited by the endothelium, derive into macrophages in the plaque, and contribute to the initiation, progression, and eventual rupture of atherosclerotic lesions (44, 45). The generation of foam cells is the initial and critical step in the development of atherosclerosis (46). Macrophages can uptake modified LDL, such as oxLDL, by a family of scavenger receptors, among which CD36 and SR-A are principal contributors to oxLDL uptake (47–49). In the current study, we found that deficiency of PXR decreased macrophage CD36 expression but did not affect the expression of SR-A and other genes regulating macrophage cholesterol efflux, including ABCA1 and ABCG1. CD36 has been shown to mediate macrophage lipid uptake and foam cell formation in vitro and in vivo (42, 50–53). Indeed, we found that PXR-deficient macrophages also had reduced lipid accumulation and foam cell formation. Consistently, PXR$^{\Delta Mye}$LDLR$^{-/-}$ mice had decreased CD36 protein levels and macrophage contents within the atherosclerotic lesions as compared with control littermates.

CD36 has been identified as a direct transcriptional target of PXR, and activation of PXR can also promote CD36-mediated hepatic lipid accumulation (54). We previously also demonstrated that activation of PXR by several ligands can increase CD36 expression and lipid accumulation in macrophages of ApoE$^{-/-}$ mice in vivo, which may contribute to the increased atherosclerotic lesions in those mice (11, 55). Consistent with the current study, PXR$^{-/-}$ApoE$^{-/-}$ mice also had decreased CD36 expression and CD36-mediated lipid uptake in macrophages (12). Interestingly, deficiency of another nuclear receptor, FXR, that is closely related to PXR, also led to reduced CD36 expression and lipid accumulation in the macrophages of LDLR$^{-/-}$ (56) or ApoE$^{-/-}$ (57) mice, which may contribute to the

decreased atherosclerosis in those mice. Therefore, it is likely that decreased atherosclerosis in PXR$^{\Delta Mye}$LDLR$^{-/-}$ mice was due, at least partially, to reduced CD36 expression and CD36-mediated lipid uptake and foam cell formation.

The role of CD36 in the regulation of atherosclerosis development has been extensively studied by several groups in multiple mouse models. CD36 has been shown to promote macrophage foam cell formation and atherosclerosis development in ApoE$^{-/-}$ mice (58), and deficiency of CD36 significantly decreased atherosclerotic lesion area at both aortic surface and aortic sinus in ApoE$^{-/-}$ mice (51, 53). Consistently, depletion of CD36 in macrophages by bone marrow translation also resulted in significantly decreased atherosclerosis in ApoE$^{-/-}$ mice and reintroduction of macrophage CD36 led to increased atherosclerosis in those mice (59). In addition to ApoE$^{-/-}$ mice, CD36 can also contribute to atherosclerosis development in LDLR$^{-/-}$ mice fed a cholesterol-enriched diet (43). Interestingly, another study found that CD36$^{-/-}$ApoE$^{-/-}$ mice had increased rather than decreased atherosclerosis in the aortic sinus areas as compared with ApoE$^{-/-}$ mice (52). Loss of CD36 and SR-A has also been shown to reduce atherosclerotic lesion complexity without affecting atherosclerotic lesion size in ApoE$^{-/-}$ mice (60). Despite the discrepancy, strong evidence suggests that CD36 plays an important role in macrophage lipid accumulation and foam cell formation in vitro and in vivo (42, 52). CD36 signaling in response to oxLDL can modulate macrophage migration and contribute to macrophage trapping in atherosclerotic lesions (61). A recent study also demonstrated that oxLDL-bound CD36 can recruit NA/K-ATPase complex in macrophages to promote atherosclerosis (62). Collectively, these studies suggest that functions of CD36 in atherosclerosis are complex, and multiple factors, such as dietary cholesterol, can affect CD36-mediated atherogenesis.

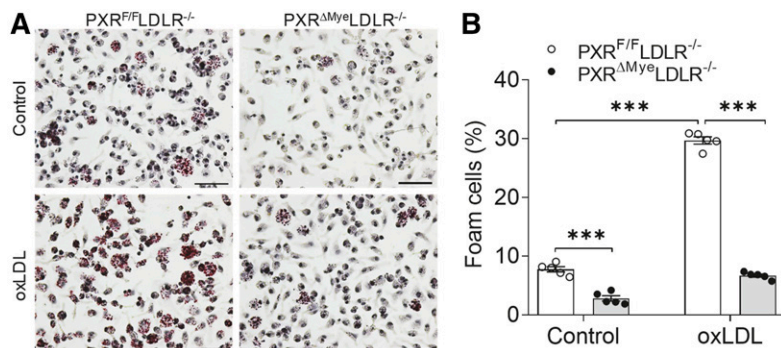**Fig. 8.** PXR-deficient macrophages have impaired lipid uptake properties. A: Freshly isolated PMs from PXR$^{F/F}$LDLR$^{-/-}$ and PXR$^{\Delta Mye}$LDLR$^{-/-}$ littermates were incubated with oxLDL (100 μg/ml) for 24 h and stained with Oil Red O and hematoxylin (scale bars, 100 μm). B: Foam cell quantification from PMs in studies described in panel A (n = 5, ***$P< 0.001$).
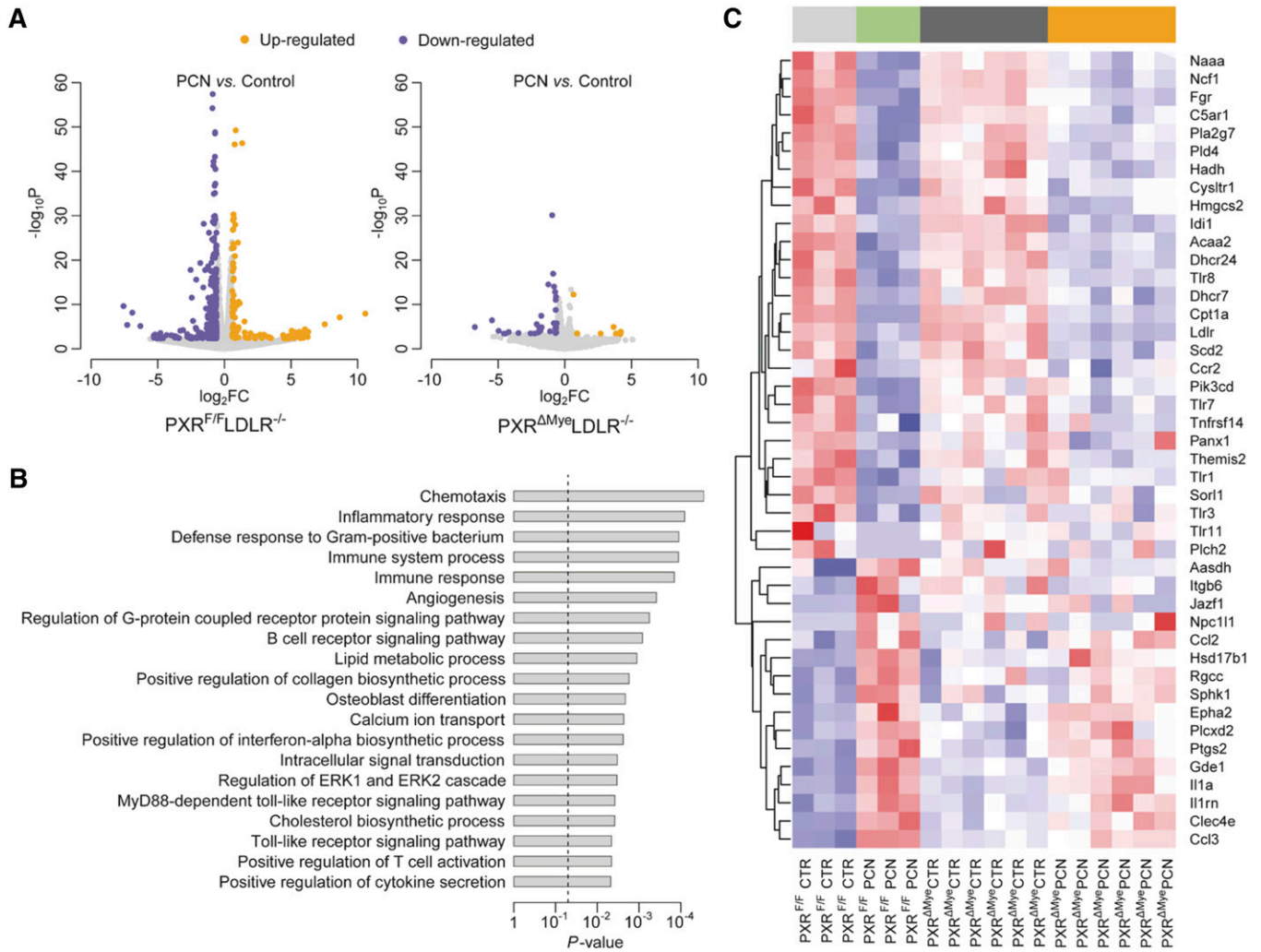
Fig. 9. PXR ligand treatment affects atherosclerosis-related gene expression in macrophages in vitro. PMs were isolated from PXR$^{F/F}$LDLR$^{-/-}$ and PXR$^{\Delta Mye}$LDLR$^{-/-}$ mice. Macrophages were treated with 20 μM of the PXR ligand, PCN, or vehicle control (DMSO) for 12 h and total RNA was isolated for RNA-Seq analysis (n = 3–6). A: Volcano plots of DEGs in control and PXR-deficient macrophages after PCN treatment. Orange dots indicate upregulation; blue dots indicate downregulation; and gray dots indicate nonsignificance relative to cut-off criteria for DEG significance. The significance threshold used was FDR of <5% and FC of >1.5. The y axis displays the $-\log_{10}$P value for each gene, while the x axis displays the $\log_2$ FC for that gene relative to control. B: The GO biological process terms significantly associated with the DEGs in control macrophages after PCN treatment. The *P*-values were computed by Fisher's exact test. The vertical dashed line indicates the significance level of α = 0.05. The y axis displays the GO biological process terms while the x axis displays the *P*-values. C: Heatmap representation of DEGs involved in the biological processes of "Lipid metabolic process," "Cholesterol biosynthetic process," "Inflammatory response," and "Positive regulation of cytokine secretion" shown in panel B. Each row shows one individual gene and each column a biological duplicate of the mouse.

Human studies have indicated a potential link between CD36 expression and atherosclerosis development. An early study on human atherosclerotic arteries showed that obese people with dyslipidemia had increased CD36 expression in macrophages within atherosclerotic plaques, whereas the CD36 expression in macrophages without atherosclerotic lesions was negligible (63). Handberg et al. (64) also found a correlation between the plasma soluble CD36 levels and carotid atherosclerosis in a human study throughout 14 European countries. Elevated soluble CD36 levels have also been detected in the monocytes of patients with coronary artery disease (65) or acute coronary syndrome (66). Future studies are required to investigate the detailed mechanisms through which the PXR-CD36 axis regulates atherosclerosis development in different animal models and possibly in humans.

In addition to CD36, we and others have previously reported that PXR can regulate multiple genes, including SCD-1, DGATs, lipin-1, Insig-1, and squalene epoxidase, that mediate lipid homeostasis in other tissues (9, 13, 14, 16, 54, 67–71). For example, we recently identified several novel transcriptional targets of PXR, including cholesterol transporter Niemann-Pick C1-like 1 (NPC1L1) and microsomal triglyceride transfer protein (MTP), that play key roles in regulating intestinal lipid absorption and lipoprotein assembly and secretion (14, 16). Interestingly, our RNA-Seq analysis of PMs treated with control or PXR ligand PCN in vitro also demonstrated that PCN treatment

can significantly affect many genes involved in lipid homeostasis in macrophages of PXR$^{F/F}$LDLR$^{-/-}$ mice but not in that PXR$^{\Delta Mye}$LDLR$^{-/-}$ mice. Consistent with our previous results from other tissues and cell types (14, 16), NPC1L1 was also upregulated by PCN-mediated PXR activation in control but not PXR-deficient macrophages. In addition to regulating cholesterol uptake by enterocytes in the gut, NPC1L1 is also expressed in human macrophages and NPC1L1 may also contribute to class B scavenger receptor (e.g., CD36)-dependent uptake of oxLDL in those macrophages (72). Therefore, it is plausible that PXR may regulate multiple pathways in macrophages that contribute to increased foam cell formation and atherosclerosis development.

It is also intriguing that CD36 expression was downregulated in PXR-deficient macrophages but was not upregulated by PCN treatment in vitro based on the RNA-Seq analysis. CD36 has been demonstrated to be regulated by multiple pathways, including LXR, PPARγ, and inflammatory signaling such as interferon-γ (73–76). For example, PPARγ is required for maintaining basal expression of CD36 in macrophages, and deficiency of PPARγ led to reduced CD36 expression in PPARγ-deficient mice (76, 77). In addition, we and others have previously demonstrated that certain PXR ligands can activate PXR and regulate its target gene expression in a tissue-specific manner (9, 16, 78, 79). Thus, PXR signaling may be important for maintaining basal CD36 expression in macrophages in vivo. However, the different in vitro environment, the selected PCN dosage, and treatment period may partially explain that unaffected CD36 expression by PCN treatment in vitro. It would be interesting to study how PXR and other signaling pathways coordinately regulate CD36 expression and the potential impact on atherosclerosis development and CVD risk in humans in the future.

In addition to those lipogenic genes, PCN-mediated PXR activation also affected inflammatory gene expression in vitro. We previously demonstrated that PXR can cross-talk with the NF-κB signaling pathway to regulate inflammatory responses (80). We have recently revealed the complex role of NF-κB signaling in atherogenesis and metabolic disorders, and found that NF-κB signaling in different cell types (e.g., myeloid, SMCs, adipocytes) may have pro- and anti-atherogenic effects (26, 29, 81, 82). In addition to NF-κB signaling, it has been reported that PXR can also regulate innate immunity by activating the NLRP3 inflammasome in other cell types, such as ECs (83). Therefore, it is plausible that PXR signaling can also regulate the NLRP3 inflammasome in macrophages and that myeloid PXR may regulate atherogenesis at multiple levels. Future studies are required to investigate the precise mechanisms through which PXR signaling regulates macrophage functions and atherosclerosis in different animal models and humans.

In summary, we generated a novel PXR$^{\Delta Mye}$LDLR$^{-/-}$ mouse model to study the role of myeloid PXR signaling in atherosclerosis. We found that myeloid-specific PXR deficiency decreased atherosclerosis in lean LDLR$^{-/-}$ mice without affecting metabolic phenotypes and lipid profile. Deficiency of PXR reduced macrophage lipid uptake and foam cell formation, which likely contribute to the decreased atherosclerosis in PXR$^{\Delta Mye}$LDLR$^{-/-}$ mice. RNA-Seq studies demonstrated that treatment with PXR ligand PCN affected atherosclerosis-related gene expression in macrophages in vitro. PXR is an important xenobiotic sensor that plays a key role in mediating xenobiotic responses. Findings from this study will hopefully stimulate further investigations of the role of PXR in macrophage biology and atherogenesis, and the perspective of PXR-mediated "gene-environment interactions" in predisposing individuals to CVD.

Data availability

The RNA-Seq datasets have been deposited in the Gene Expression Omnibus (GSE145719). Data that support the plots within this publication and other findings of this study are available from the corresponding author upon request.

REFERENCES

1. Roth, G. A., M. H. Forouzanfar, A. E. Moran, R. Barber, G. Nguyen, V. L. Feigin, M. Naghavi, G. A. Mensah, and C. J. Murray. 2015. Demographic and epidemiologic drivers of global cardiovascular mortality. *N. Engl. J. Med.* **372:** 1333–1341.
2. Robinson-Rechavi, M., A. S. Carpentier, M. Duffraisse, and V. Laudet. 2001. How many nuclear hormone receptors are there in the human genome? *Trends Genet.* **17:** 554–556.
3. Mangelsdorf, D. J., C. Thummel, M. Beato, P. Herrlich, G. Schutz, K. Umesono, B. Blumberg, P. Kastner, M. Mark, P. Chambon, et al. 1995. The nuclear receptor superfamily: the second decade. *Cell.* **83:** 835–839.
4. Barish, G. D., and R. M. Evans. 2004. PPARs and LXRs: atherosclerosis goes nuclear. *Trends Endocrinol. Metab.* **15:** 158–165.
5. Glass, C. K. 2006. Going nuclear in metabolic and cardiovascular disease. *J. Clin. Invest.* **116:** 556–560.
6. Blumberg, B., W. Sabbagh, Jr., H. Juguilon, J. Bolado, Jr., C. M. van Meter, E. S. Ong, and R. M. Evans. 1998. SXR, a novel steroid and xenobiotic-sensing nuclear receptor. *Genes Dev.* **12:** 3195–3205.
7. Kliewer, S. A., B. Goodwin, and T. M. Willson. 2002. The nuclear pregnane X receptor: a key regulator of xenobiotic metabolism. *Endocr. Rev.* **23:** 687–702.
8. Zhou, C., S. Verma, and B. Blumberg. 2009. The steroid and xenobiotic receptor (SXR), beyond xenobiotic metabolism. *Nucl. Recept. Signal.* **7:** e001.
9. Zhou, C. 2016. Novel functions of PXR in cardiometabolic disease. *Biochim. Biophys. Acta.* **1859:** 1112–1120.
10. Blumberg, B., and R. M. Evans. 1998. Orphan nuclear receptors–new ligands and new possibilities. *Genes Dev.* **12:** 3149–3155.
11. Zhou, C., N. King, K. Y. Chen, and J. L. Breslow. 2009. Activation of PXR induces hypercholesterolemia in wild-type and accelerates atherosclerosis in apoE deficient mice. *J. Lipid Res.* **50:** 2004–2013.
12. Sui, Y., J. Xu, J. Rios-Pilier, and C. Zhou. 2011. Deficiency of PXR decreases atherosclerosis in apoE-deficient mice. *J. Lipid Res.* **52:** 1652–1659.
13. Gwag, T., Z. Meng, Y. Sui, R. N. Helsley, S. H. Park, S. Wang, R. N. Greenberg, and C. Zhou. 2019. Non-nucleoside reverse transcriptase inhibitor efavirenz activates PXR to induce hypercholesterolemia and hepatic steatosis. *J. Hepatol.* **70:** 930–940.
14. Meng, Z., T. Gwag, Y. Sui, S. H. Park, X. Zhou, and C. Zhou. 2019. The atypical antipsychotic quetiapine induces hyperlipidemia by activating intestinal PXR signaling. *JCI Insight.* **4:** e125657.
15. Helsley, R. N., Y. Sui, N. Ai, S. H. Park, W. J. Welsh, and C. Zhou. 2013. Pregnane X receptor mediates dyslipidemia induced by the HIV protease inhibitor amprenavir in mice. *Mol. Pharmacol.* **83:** 1190–1199.

16. Sui, Y., R. N. Helsley, S. H. Park, X. Song, Z. Liu, and C. Zhou. 2015. Intestinal pregnane x receptor links xenobiotic exposure and hypercholesterolemia. *Mol. Endocrinol.* **29:** 765–776.

17. Dubrac, S., A. Elentner, S. Ebner, J. Horejs-Hoeck, and M. Schmuth. 2010. Modulation of T lymphocyte function by the pregnane X receptor. *J. Immunol.* **184:** 2949–2957.

18. Albermann, N., F. H. Schmitz-Winnenthal, K. Z'graggen, C. Volk, M. M. Hoffmann, W. E. Haefeli, and J. Weiss. 2005. Expression of the drug transporters MDR1/ABCB1, MRP1/ABCC1, MRP2/ABCC2, BCRP/ABCG2, and PXR in peripheral blood mononuclear cells and their relationship with the expression in intestine and liver. *Biochem. Pharmacol.* **70:** 949–958.

19. Owen, A., B. Chandler, D. J. Back, and S. H. Khoo. 2004. Expression of pregnane-X-receptor transcript in peripheral blood mononuclear cells and correlation with MDR1 mRNA. *Antivir. Ther.* **9:** 819–821.

20. Siest, G., E. Jeannesson, J. B. Marteau, A. Samara, B. Marie, M. Pfister, and S. Visvikis-Siest. 2008. Transcription factor and drug-metabolizing enzyme gene expression in lymphocytes from healthy human subjects. *Drug Metab. Dispos.* **36:** 182–189.

21. Casey, S. C., and B. Blumberg. 2012. The steroid and xenobiotic receptor negatively regulates B-1 cell development in the fetal liver. *Mol. Endocrinol.* **26:** 916–925.

22. Casey, S. C., E. L. Nelson, G. M. Turco, M. R. Janes, D. A. Fruman, and B. Blumberg. 2011. B-1 cell lymphoma in mice lacking the steroid and xenobiotic receptor, SXR. *Mol. Endocrinol.* **25:** 933–943.

23. Lusis, A. J. 2000. Atherosclerosis. *Nature.* **407:** 233–241.

24. Glass, C. K., and J. L. Witztum. 2001. Atherosclerosis. the road ahead. *Cell.* **104:** 503–516.

25. Clausen, B. E., C. Burkhardt, W. Reith, R. Renkawitz, and I. Forster. 1999. Conditional gene targeting in macrophages and granulocytes using LysMcre mice. *Transgenic Res.* **8:** 265–277.

26. Park, S. H., Y. Sui, F. Gizard, J. Xu, J. Rios-Pilier, R. N. Helsley, S. S. Han, and C. Zhou. 2012. Myeloid-specific IkappaB kinase beta deficiency decreases atherosclerosis in low-density lipoprotein receptor-deficient mice. *Arterioscler. Thromb. Vasc. Biol.* **32:** 2869–2876.

27. Teupser, D., A. D. Persky, and J. L. Breslow. 2003. Induction of atherosclerosis by low-fat, semisynthetic diets in LDL receptor-deficient C57BL/6J and FVB/NJ mice: comparison of lesions of the aortic root, brachiocephalic artery, and whole aorta (en face measurement). *Arterioscler. Thromb. Vasc. Biol.* **23:** 1907–1913.

28. Wolfrum, S., D. Teupser, M. Tan, K. Y. Chen, and J. L. Breslow. 2007. The protective effect of A20 on atherosclerosis in apolipoprotein E-deficient mice is associated with reduced expression of NF-kappaB target genes. *Proc. Natl. Acad. Sci. USA.* **104:** 18601–18606.

29. Sui, Y., S. H. Park, J. Xu, S. Monette, R. N. Helsley, S. S. Han, and C. Zhou. 2014. IKKbeta links vascular inflammation to obesity and atherosclerosis. *J. Exp. Med.* **211:** 869–886.

30. Helsley, R. N., Y. Sui, S. H. Park, Z. Liu, R. G. Lee, B. Zhu, P. A. Kern, and C. Zhou. 2016. Targeting IkappaB kinase beta in adipocyte lineage cells for treatment of obesity and metabolic dysfunctions. *Stem Cells.* **34:** 1883–1895.

31. Wang, F., Z. Liu, S. H. Park, T. Gwag, W. Lu, M. Ma, Y. Sui, and C. Zhou. 2018. Myeloid beta-catenin deficiency exacerbates atherosclerosis in low-density lipoprotein receptor-deficient mice. *Arterioscler. Thromb. Vasc. Biol.* **38:** 1468–1478.

32. Sui, Y., S. H. Park, F. Wang, and C. Zhou. 2018. Perinatal bisphenol A exposure increases atherosclerosis in adult male PXR-humanized mice. *Endocrinology.* **159:** 1595–1608.

33. Zhong, S., J. G. Joung, Y. Zheng, Y. R. Chen, B. Liu, Y. Shao, J. Z. Xiang, Z. Fei, and J. J. Giovannoni. 2011. High-throughput Illumina strand-specific RNA sequencing library preparation. *Cold Spring Harb. Protoc.* **2011:** 940–949.

34. Levin, J. Z., M. Yassour, X. Adiconis, C. Nusbaum, D. A. Thompson, N. Friedman, A. Gnirke, and A. Regev. 2010. Comprehensive comparative analysis of strand-specific RNA sequencing methods. *Nat. Methods.* **7:** 709–715.

35. Patro, R., S. M. Mount, and C. Kingsford. 2014. Sailfish enables alignment-free isoform quantification from RNA-seq reads using lightweight algorithms. *Nat. Biotechnol.* **32:** 462–464.

36. Zhao, S., and B. Zhang. 2015. A comprehensive evaluation of Ensembl, RefSeq, and UCSC annotations in the context of RNA-seq read mapping and gene quantification. *BMC Genomics.* **16:** 97.

37. Robinson, M. D., D. J. McCarthy, and G. K. Smyth. 2010. edgeR: a Bioconductor package for differential expression analysis of digital gene expression data. *Bioinformatics.* **26:** 139–140.

38. Ashburner, M., C. A. Ball, J. A. Blake, D. Botstein, H. Butler, J. M. Cherry, A. P. Davis, K. Dolinski, S. S. Dwight, J. T. Eppig, et al.

39. 2000. Gene ontology: tool for the unification of biology. The Gene Ontology Consortium. *Nat. Genet.* **25:** 25–29.

39. Sui, Y., Z. Liu, S. H. Park, S. E. Thatcher, B. Zhu, J. P. Fernandez, H. Molina, P. A. Kern, and C. Zhou. 2018. IKKβ is a β-catenin kinase that regulates mesenchymal stem cell differentiation. *JCI Insight.* **3:** 96660.

40. Rao, X., J. Zhong, A. Maiseyeu, B. Gopalakrishnan, F. A. Villamena, L. C. Chen, J. R. Harkema, Q. Sun, and S. Rajagopalan. 2014. CD36-dependent 7-ketocholesterol accumulation in macrophages mediates progression of atherosclerosis in response to chronic air pollution exposure. *Circ. Res.* **115:** 770–780.

41. Zhou, C., B. Pridgen, N. King, J. Xu, and J. L. Breslow. 2011. Hyperglycemic Ins2AkitaLdlr-/- mice show severely elevated lipid levels and increased atherosclerosis: a model of type 1 diabetic macrovascular disease. *J. Lipid Res.* **52:** 1483–1493.

42. Rahaman, S. O., D. J. Lennon, M. Febbraio, E. A. Podrez, S. L. Hazen, and R. L. Silverstein. 2006. A CD36-dependent signaling cascade is necessary for macrophage foam cell formation. *Cell Metab.* **4:** 211–221.

43. Kennedy, D. J., S. D. Kuchibhotla, E. Guy, Y. M. Park, G. Nimako, D. Vanegas, R. E. Morton, and M. Febbraio. 2009. Dietary cholesterol plays a role in CD36-mediated atherogenesis in LDLR-knockout mice. *Arterioscler. Thromb. Vasc. Biol.* **29:** 1481–1487.

44. Hansson, G. K., and A. Hermansson. 2011. The immune system in atherosclerosis. *Nat. Immunol.* **12:** 204–212.

45. Hamers, A. A., M. Vos, F. Rassam, G. Marinkovic, K. Kurakula, P. J. van Gorp, M. P. de Winther, M. J. Gijbels, V. de Waard, and C. J. de Vries. 2012. Bone marrow-specific deficiency of nuclear receptor Nur77 enhances atherosclerosis. *Circ. Res.* **110:** 428–438. [Erratum. 2012. *Circ. Res.* 110: e46.]

46. Stary, H. C., A. B. Chandler, S. Glagov, J. R. Guyton, W. Insull, Jr., M. E. Rosenfeld, S. A. Schaffer, C. J. Schwartz, W. D. Wagner, and R. W. Wissler. 1994. A definition of initial, fatty streak, and intermediate lesions of atherosclerosis. A report from the Committee on Vascular Lesions of the Council on Arteriosclerosis, American Heart Association. *Circulation.* **89:** 2462–2478.

47. de Villiers, W. J., and E. J. Smart. 1999. Macrophage scavenger receptors and foam cell formation. *J. Leukoc. Biol.* **66:** 740–746.

48. Kunjathoor, V. V., M. Febbraio, E. A. Podrez, K. J. Moore, L. Andersson, S. Koehn, J. S. Rhee, R. Silverstein, H. F. Hoff, and M. W. Freeman. 2002. Scavenger receptors class A-I/II and CD36 are the principal receptors responsible for the uptake of modified low density lipoprotein leading to lipid loading in macrophages. *J. Biol. Chem.* **277:** 49982–49988.

49. Collot-Teixeira, S., J. Martin, C. McDermott-Roe, R. Poston, and J. L. McGregor. 2007. CD36 and macrophages in atherosclerosis. *Cardiovasc. Res.* **75:** 468–477.

50. Abumrad, N. A., M. R. el-Maghrabi, E. Z. Amri, E. Lopez, and P. A. Grimaldi. 1993. Cloning of a rat adipocyte membrane protein implicated in binding or transport of long-chain fatty acids that is induced during preadipocyte differentiation. Homology with human CD36. *J. Biol. Chem.* **268:** 17665–17668.

51. Febbraio, M., E. A. Podrez, J. D. Smith, D. P. Hajjar, S. L. Hazen, H. F. Hoff, K. Sharma, and R. L. Silverstein. 2000. Targeted disruption of the class B scavenger receptor CD36 protects against atherosclerotic lesion development in mice. *J. Clin. Invest.* **105:** 1049–1056.

52. Moore, K. J., V. V. Kunjathoor, S. L. Koehn, J. J. Manning, A. A. Tseng, J. M. Silver, M. McKee, and M. W. Freeman. 2005. Loss of receptor-mediated lipid uptake via scavenger receptor A or CD36 pathways does not ameliorate atherosclerosis in hyperlipidemic mice. *J. Clin. Invest.* **115:** 2192–2201.

53. Guy, E., S. Kuchibhotla, R. Silverstein, and M. Febbraio. 2007. Continued inhibition of atherosclerotic lesion development in long term Western diet fed CD36o /apoEo mice. *Atherosclerosis.* **192:** 123–130.

54. Zhou, J., Y. Zhai, Y. Mu, H. Gong, H. Uppal, D. Toma, S. Ren, R. M. Evans, and W. Xie. 2006. A novel pregnane X receptor-mediated and sterol regulatory element-binding protein-independent lipogenic pathway. *J. Biol. Chem.* **281:** 15013–15020.

55. Sui, Y., S. H. Park, R. N. Helsley, M. Sunkara, F. J. Gonzalez, A. J. Morris, and C. Zhou. 2014. Bisphenol A increases atherosclerosis in pregnane X receptor-humanized ApoE deficient mice. *J. Am. Heart Assoc.* **3:** e000492.

56. Zhang, Y., X. Wang, C. Vales, F. Y. Lee, H. Lee, A. J. Lusis, and P. A. Edwards. 2006. FXR deficiency causes reduced atherosclerosis in Ldlr-/- mice. *Arterioscler. Thromb. Vasc. Biol.* **26:** 2316–2321.

57. Guo, G. L., S. Santamarina-Fojo, T. E. Akiyama, M. J. Amar, B. J. Paigen, B. Brewer, Jr., and F. J. Gonzalez. 2006. Effects of FXR in foam-cell formation and atherosclerosis development. *Biochim. Biophys. Acta.* **1761:** 1401–1409.

58. Febbraio, M., D. P. Hajjar, and R. L. Silverstein. 2001. CD36: a class B scavenger receptor involved in angiogenesis, atherosclerosis, inflammation, and lipid metabolism. *J. Clin. Invest.* **108:** 785–791.

59. Febbraio, M., E. Guy, and R. L. Silverstein. 2004. Stem cell transplantation reveals that absence of macrophage CD36 is protective against atherosclerosis. *Arterioscler. Thromb. Vasc. Biol.* **24:** 2333–2338.

60. Manning-Tobin, J. J., K. J. Moore, T. A. Seimon, S. A. Bell, M. Sharuk, J. I. Alvarez-Leite, M. P. de Winther, I. Tabas, and M. W. Freeman. 2009. Loss of SR-A and CD36 activity reduces atherosclerotic lesion complexity without abrogating foam cell formation in hyperlipidemic mice. *Arterioscler. Thromb. Vasc. Biol.* **29:** 19–26.

61. Park, Y. M., M. Febbraio, and R. L. Silverstein. 2009. CD36 modulates migration of mouse and human macrophages in response to oxidized LDL and may contribute to macrophage trapping in the arterial intima. *J. Clin. Invest.* **119:** 136–145.

62. Chen, Y., D. J. Kennedy, D. P. Ramakrishnan, M. Yang, W. Huang, Z. Li, Z. Xie, A. C. Chadwick, D. Sahoo, and R. L. Silverstein. 2015. Oxidized LDL-bound CD36 recruits an Na(+)/K(+)-ATPase-Lyn complex in macrophages that promotes atherosclerosis. *Sci. Signal.* **8:** ra91.

63. Nakata, A., Y. Nakagawa, M. Nishida, S. Nozaki, J. Miyagawa, T. Nakagawa, R. Tamura, K. Matsumoto, K. Kameda-Takemura, S. Yamashita, et al. 1999. CD36, a novel receptor for oxidized low-density lipoproteins, is highly expressed on lipid-laden macrophages in human atherosclerotic aorta. *Arterioscler. Thromb. Vasc. Biol.* **19:** 1333–1339.

64. Handberg, A., K. Hojlund, A. Gastaldelli, A. Flyvbjerg, J. M. Dekker, J. Petrie, P. Piatti, H. Beck-Nielsen, and R. Investigators. 2012. Plasma sCD36 is associated with markers of atherosclerosis, insulin resistance and fatty liver in a nondiabetic healthy population. *J. Intern. Med.* **271:** 294–304.

65. Teupser, D., M. A. Mueller, J. Koglin, W. Wilfert, J. Ernst, W. von Scheidt, G. Steinbeck, D. Seidel, and J. Thiery. 2008. CD36 mRNA expression is increased in CD14+ monocytes of patients with coronary heart disease. *Clin. Exp. Pharmacol. Physiol.* **35:** 552–556.

66. Piechota, M., A. Banaszewska, J. Dudziak, M. Slomczynski, and R. Plewa. 2012. Highly upregulated expression of CD36 and MSR1 in circulating monocytes of patients with acute coronary syndromes. *Protein J.* **31:** 511–518.

67. He, J., J. Gao, M. Xu, S. Ren, M. Stefanovic-Racic, R. M. O'Doherty, and W. Xie. 2013. PXR ablation alleviates diet-induced and genetic obesity and insulin resistance in mice. *Diabetes.* **62:** 1876–1887.

68. Moreau, A., C. Teruel, M. Beylot, V. Albalea, V. Tamasi, T. Umbdenstock, Y. Parmentier, A. Sa-Cunha, B. Suc, J. M. Fabre, et al. 2009. A novel pregnane X receptor and S14-mediated lipogenic pathway in human hepatocyte. *Hepatology.* **49:** 2068–2079.

69. Roth, A., R. Looser, M. Kaufmann, S. Blaettler, F. Rencurel, W. Huang, D. D. Moore, and U. A. Meyer. 2008. Regulatory cross-talk between drug metabolism and lipid homeostasis: constitutive androstane receptor and pregnane X receptor increase Insig-1 expression. *Mol. Pharmacol.* **73:** 1282–1289.

70. Nakamura, K., R. Moore, M. Negishi, and T. Sueyoshi. 2007. Nuclear pregnane X receptor cross-talk with FoxA2 to mediate drug-induced regulation of lipid metabolism in fasting mouse liver. *J. Biol. Chem.* **282:** 9768–9776.

71. Bachmanov, A. A., D. R. Reed, G. K. Beauchamp, and M. G. Tordoff. 2002. Food intake, water intake, and drinking spout side preference of 28 mouse strains. *Behav. Genet.* **32:** 435–443.

72. Seedorf, U., T. Engel, A. Lueken, G. Bode, S. Lorkowski, and G. Assmann. 2004. Cholesterol absorption inhibitor Ezetimibe blocks uptake of oxidized LDL in human macrophages. *Biochem. Biophys. Res. Commun.* **320:** 1337–1341.

73. Zhou, J., M. Febbraio, T. Wada, Y. Zhai, R. Kuruba, J. He, J. H. Lee, S. Khadem, S. Ren, S. Li, et al. 2008. Hepatic fatty acid transporter Cd36 is a common target of LXR, PXR, and PPARgamma in promoting steatosis. *Gastroenterology.* **134:** 556–567.

74. Han, J., D. P. Hajjar, J. M. Tauras, J. Feng, A. M. Gotto, Jr., and A. C. Nicholson. 2000. Transforming growth factor-beta1 (TGF-beta1) and TGF-beta2 decrease expression of CD36, the type B scavenger receptor, through mitogen-activated protein kinase phosphorylation of peroxisome proliferator-activated receptor-gamma. *J. Biol. Chem.* **275:** 1241–1246.

75. Yesner, L. M., H. Y. Huh, S. F. Pearce, and R. L. Silverstein. 1996. Regulation of monocyte CD36 and thrombospondin-1 expression by soluble mediators. *Arterioscler. Thromb. Vasc. Biol.* **16:** 1019–1025.

76. Moore, K. J., E. D. Rosen, M. L. Fitzgerald, F. Randow, L. P. Andersson, D. Altshuler, D. S. Milstone, R. M. Mortensen, B. M. Spiegelman, and M. W. Freeman. 2001. The role of PPAR-gamma in macrophage differentiation and cholesterol uptake. *Nat. Med.* **7:** 41–47.

77. Akiyama, T. E., S. Sakai, G. Lambert, C. J. Nicol, K. Matsusue, S. Pimprale, Y. H. Lee, M. Ricote, C. K. Glass, H. B. Brewer, Jr., et al. 2002. Conditional disruption of the peroxisome proliferator-activated receptor gamma gene in mice results in lowered expression of ABCA1, ABCG1, and apoE in macrophages and reduced cholesterol efflux. *Mol. Cell. Biol.* **22:** 2607–2619.

78. Zhou, C., M. M. Tabb, A. Sadatrafiei, F. Grun, and B. Blumberg. 2004. Tocotrienols activate the steroid and xenobiotic receptor, SXR, and selectively regulate expression of its target genes. *Drug Metab. Dispos.* **32:** 1075–1082.

79. Cheng, J., Y. M. Shah, X. Ma, X. Pang, T. Tanaka, T. Kodama, K. W. Krausz, and F. J. Gonzalez. 2010. Therapeutic role of rifaximin in inflammatory bowel disease: clinical implication of human pregnane X receptor activation. *J. Pharmacol. Exp. Ther.* **335:** 32–41.

80. Zhou, C., M. M. Tabb, E. L. Nelson, F. Grun, S. Verma, A. Sadatrafiei, M. Lin, S. Mallick, B. M. Forman, K. E. Thummel, et al. 2006. Mutual repression between steroid and xenobiotic receptor and NF-kappaB signaling pathways links xenobiotic metabolism and inflammation. *J. Clin. Invest.* **116:** 2280–2289.

81. Park, S. H., Z. Liu, Y. Sui, R. N. Helsley, B. Zhu, D. K. Powell, P. A. Kern, and C. Zhou. 2016. IKKbeta is essential for adipocyte survival and adaptive adipose remodeling in obesity. *Diabetes.* **65:** 1616–1629.

82. Lu, W., S. H. Park, Z. Meng, F. Wang, and C. Zhou. 2019. Deficiency of adipocyte IKKbeta affects atherosclerotic plaque vulnerability in obese LDLR deficient mice. *J. Am. Heart Assoc.* **8:** e012009.

83. Wang, S., T. Lei, K. Zhang, W. Zhao, L. Fang, B. Lai, J. Han, L. Xiao, and N. Wang. 2014. Xenobiotic pregnane X receptor (PXR) regulates innate immunity via activation of NLRP3 inflammasome in vascular endothelial cells. *J. Biol. Chem.* **289:** 30075–30081.